Temperature Distribution for a Friction Taper Stud Weld in Thick Walled 10CrMo910 Steel

D.G. Hattingh[a] and C. van Zyl[b]

Received 8 August 2011, in revised form 12 August 2012 and accepted 30 October 2012

Heat distribution by direct measurement, as a function of weld time and position, during friction taper stud welding (FTSW) in 10CrMo910 thick wall steam pipe coupon is investigated. As expected, the main hotspots during welding were identified to be close to the top surface just before weld completion and at the bottom centre surface of the plug weld at the interface line. The maximum temperature of 1102 °C was recorded at the tool hole interface within 3 s after the start of the weld. This corresponds to the initial "dry friction" stage where the heat generation initiates due to friction between the tool and parent plate. The weld power calculated from motor torque increases rapidly at the start of the weld and reached a peak value after 8 s, while a temperature of 964 °C was reached after 34 s, at the top edge of the weld. This position of the second peak temperature are most probably the result of heat transferred together with the accumulation of expelled material forming on the surface of the parent plate during the FTSW process.

Additional keywords: Thermocouple, heat transfer, solid state, thermal profile, forging, ferritic, creep resistant steel, third body.

1. Introduction

The concept of friction welding is widely accepted as a process based on the conversion of mechanical work to thermal energy to provide conditions suitable for joining or processing, which has for the past five decades, mainly been applied to round bars. During friction processing the parts are typically subjected to solid contact friction during the initial stage, but rapidly, as heat is generated, the material plasticises into a 'third-body' layer.

Once plasticisation occurs it must be accepted that theory of basic friction no longer applies as the plasticised metal cannot transmit sufficient stress to convert mechanical work into thermal energy[1]. The interdependency of the plastic deformation, heat dissipation as a result of the frictional and viscous heat generation involved in the friction welding process, complicate the efforts to develop predictive models of the process. The prediction of accurate temperature profiles at the weld interface is difficult due to the temperature increase during the friction stage and the non-uniform heating of the contact surfaces [2,3].

Friction taper stud welding (FTSW) is an innovative solid phase welding process, developed by TWI from the concepts of friction hydro pillar processing (FHPP), which operate at lower temperatures than electrical arc welding with a less severe thermal cycle[2]. Minimal documented studies could be found on either the FHPP and/or FTSW, but reports from GKSS *Forschungszentrum* in Germany and the welding institute (TWI) showed the possible potential of the processes[5-7]. FTSW was developed to address the process limitations of FHPP on diameter and burn-off length of the consumable tool, as reported[8]. It was suggested that the tapered hole and tool, applied during FTSW, would alleviate the sudden changes in microstructure experienced during high spindle speed, high displacement welds using the FHPP[7] . A further advantage of the tapered approach in FTSW is that higher process temperatures could be reached, due to the resultant extension of the weld time, thus enabling the process to be considered for a wider range of materials[9] .

During the FTSW process a tapered hole, together with a tapered consumable, enables hydrodynamic forces to be exploited in making the joint. The tapered hole and consumable plug give an increasing cross-sectional area towards the surface and provide a nominal amount of sidewall reactive support, while the increasing cross-sectional area provides a corresponding increase in strength[10]. The consumable tool is rotated in a pre-drilled hole, under an axial load. The joining process commence when the rotating tool generates enough frictional heat at the bottom of the hole to allow for plasticisation and fusion. From frictional heat the tool and a narrow boundary region of the parent material begin to plasticise, with the tool plasticising across the complete bore of the hole[11]. The frictional surface moves up the hole filling it with plasticised metal as schematically illustrated in figure 1. Figure 2 shows a typical macrostructure formed during overlap FTSW on creep resistant steel[12] . Complete bonding between the surface of the hole and the plasticised material is developed.

After the hole is filled, the actual friction welding procedure terminates. This process lends itself for doing repair with dissimilar tool materials for improved metallurgical properties. Work has been reported on the application related to repair of undersea structures, pipelines and localised thick walled steel components [8, 13].

a MSAIMechE, Professor, eNtsa, School of Engineering, Nelson Mandela Metropolitan University, E-mail: danie.hattingh@nmmu.ac.za

b MSAIMechE, Department of Mechanical Engineering, Nelson Mandela Metropolitan University (NMMU)

http://www.saimeche.org.za (open access) © SAIMechE All rights reserved.

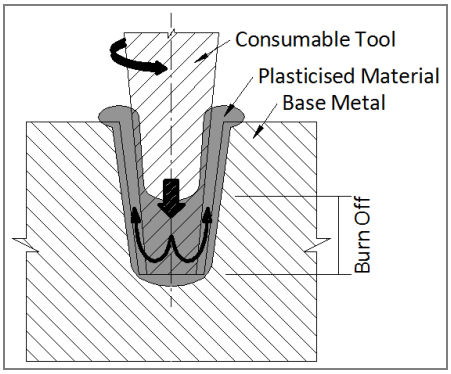

Figure 1: FTSW: Schematic flow of plasticised material of a typical FTSW



Figure 2: Typical Macrostructure of the 6 overlapping FTSW in 13CrMo44 plate[12]

FTSW results in localized modification of the material properties and hence, by understanding the thermo-mechanics involved, knowledge is contributed explaining the complex relationship between the interaction of process parameters and material properties which occur as a result of certain process parameter combinations. Heat generation during the FTSW process plays an important role in determining the mechanical properties of the weld as well as peak residual stresses after welding. Controlling the process parameters (rotational speed, duration of the weld and frictional/ forging forces (both magnitude and duration)) together with the qualitative factors (surface condition, bulk material, etc.) is of importance as these factors control the mechanisms involved at the different temperature levels, influencing the integrity of the weld[14]. It has been suggested that the weld interface temperature be used as a parameter to control the energy input to the friction weld[3] . This thermal profile has a direct influence on the bonding at the weld interface. The location and maximum temperatures reached within the base material, during the FTSW process, are thus an area of interest.

This research work relates to creep resistant 10CrMo910 pipe sections for which no published temperature data relating to FTSW currently exists. Further, during a literature search, no evidence of recorded temperature data could be found for any steel where the FTSW process was applied. Due to the inherent process and resultant differences between FTSW and friction welding in general, it is of no value to compare the temperature profiles. The data collected during this research will create an understanding of the temperature range for a given set of weld parameters by placing thermocouples at various locations around the pre drilled taper hole, an approach that have been applied to friction welding by various researchers [15, 16].

2. Experimental Background

2.1 Material

10CrMo910 a creep resistant low alloy ferritic steel (BS EN 10216 part 2) used in seamless pipe for steam conditions reaching temperatures up to about 550 °C were used as material for both the test coupon and consumable tool. The plate is supplied in a normalised and tempered condition to give a grain size of around 200 µm. This steel is mainly used in pressure part applications in boilers fired by fossil fuels and also in heat recovery system generators (HRSG). Specifically, these are tubing alloys particularly for the cooler sections of super heaters and re-heaters and also for the water walls in the temperature range where mild steel becomes too weak to withstand creep damage. Alloys of this type are also used in thick-section components such as headers and steam pipes.

The reported solidus temperature for 10CrMo910 steel is 1420 °C and melting temperature 1500 °C[17] . 10CrMo910 steel, corresponds approximately to grade T22 of ASTM A 199, 200 and 213 as well as grade P 22 of ASTM A 335 and DIN 17175, and contains the alloy elements (w-%) as indicated in table 1[18] .

2.2 Sample Preparation

A test coupon of thick walled 10CrMo910 steel pipe (OD 167.5 mm, ID 87.5 mm) was machined according to the configuration given in figure 3. A consumable tool matching the approximate hole geometry was manufactured from the same material as the test block and used to fill the hole by friction processing as shown in figure 4. To accommodate thermal process mapping, twenty nine 1.5 mm diameter holes were machined by electro discharge machining (EDM), into the block at predetermined positions and precise depth to allow for accurate positioning of 1 mm, type N thermocouples. The distribution and configuration of the holes (thermo-wells) on the centre line of the test coupon are indicated in figure 5. Temperatures were measured, at the various depths and positions, radially around the weld in real time during the actual welding process.

w-%	C	Cr	Cu	Mo	N	Si	Mn	P	S
Specification	0.08-0.14	2,0-2.5	0.3max	0.9-1.1	0.012	0.5max	0.4-0.9	0.02	0.01

Table1: Chemical composition as specified for 10CrMo910 steel

http://www.saimeche.org.za (open access) © SAIMechE All rights reserved.

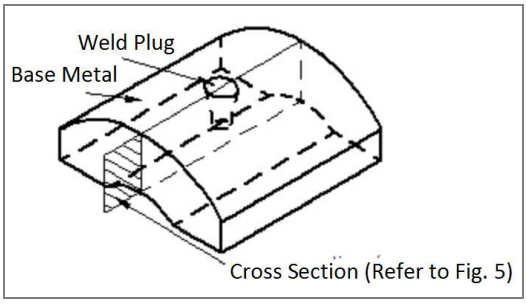

Figure 3: Typical test piece geometry



Figure 4: Welded coupon with tool shank still in place

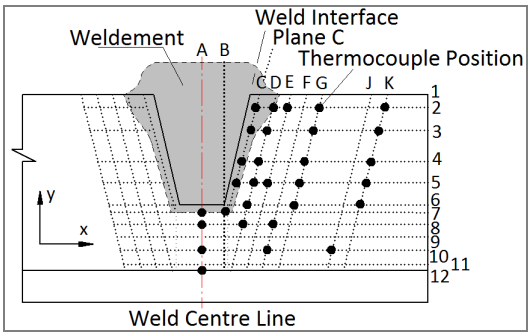

Figure 5: Cross-section showing a two-dimensional graphical representation of measurement positions

2.3 Thermocouple qualification

All thermocouples were subjected to standard testing confirming operation prior to use.

2.3.1 Calibration

The thermocouples were placed in a calibrated furnace preset to specific temperatures and left until steady temperatures were reached, after which the temperatures, measured by the thermocouples and shown by the furnace, were recorded. An average temperature, as recorded by the thermocouples, at each set temperature, was determined and compared to the average set temperature of the furnace. These values were used to determine the percentage error of the thermocouples and are graphically presented in figure 6. A function for the thermocouple error % was established and the measured temperatures subsequently adjusted prior to reporting.

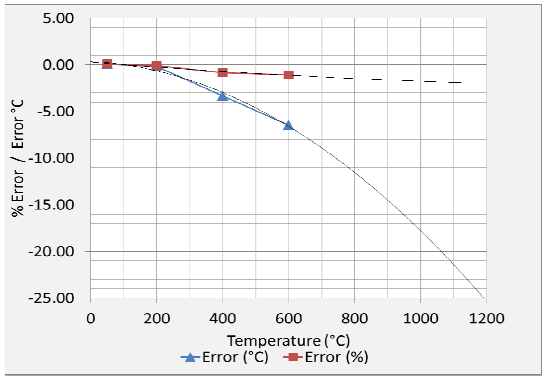

Figure 6: Thermocouple Error

2.3.2 Time constant

The time constant is defined as the time required for the sensor to reach 63.2 % of its total output signal when subjected to a step change in temperature, under set conditions. As this time constant can vary, depending on the heat transfer taking place at the point or tip of the thermocouple and the nature of the contact resistance involved, the time constant for the thermocouples being used, was experimentally determined, with the results shown in figure 7, and used to make the necessary adjustments to measured temperatures enabling determination of the instantaneous temperature of the material being tested.

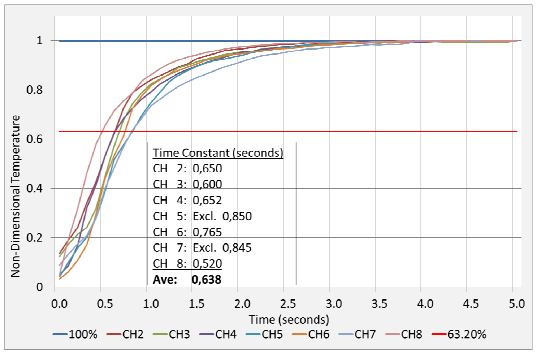

Figure 7: Transient non-dimensional temperature results

2.4 Temperature measurement

Testing was conducted on a portable Friction Stud Welding Machine developed by the NMMU[19]. Temperature data collection via 1 mm diameter type N thermocouples embedded in the test piece was done with a DataTaker DT800 data logger connected to a computer via an RS-232 cable with DeLogger 4V4R1 data logging software. The process controls were set up in such a way that weld cycle time was a function of the plunge depth with the welding duration in the order of 30 s. The thermocouples were placed inside the base metal, at different planes (A to K) from the weld centre line and levels (1 – 12) from the top surface, radially around the tapered hole as illustrated in figure 8. The temperature measurement positions, as a distance from the centre of the weld and the weld interface, are tabulated in table 2, also showing the *x* and *y* coordinates of each measuring point.

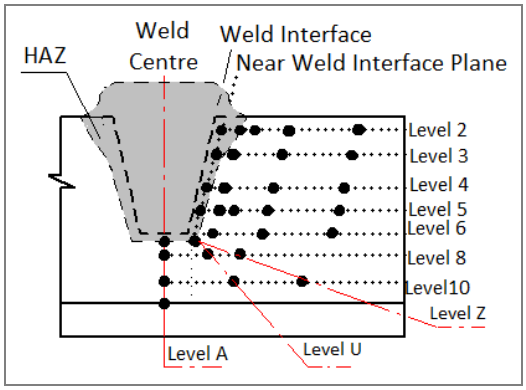

Figure 8: Temperature measurement levels

2.4 FTSW of test coupon

The FTSW platform is software controlled and there are 5 main steps in the welding procedure. To ensure maximum control and repeatability on heat input the spindle moves down and identifies the exact bottom of the hole by sensing a pressure increase when the tool touches the bottom. The tool then retracts 1 mm and awaits the start command. At this point the spindle speed is increased to 5000 rpm without making frictional contact. At reaching the selected process speed an axial load of 17.5 kN is applied for a given plunge depth. The spindle speed and down-force is kept constant until the set plunge is reached. Rotation is stopped and an axial load (Forging pressure) is applied for a specified period[8]. For this experiment the sample was produced

Plane and level of Measuring Point	K2	E2	C2	G3	C3	G4	C4	K5	E5	C5
Dim from Centre of Weld (mm) : x	34.3	17.2	11.2	22.6	10.7	21.2	9.2	32.1	14	8.4
Dim from Level 1 (mm) : y	-3	-3	-3	-8	-8	-15	-15	-20	-20	-20
Dim from Weld Interface (mm)	25.5	8.4	2.4	14.6	2.7	14.4	2.4	26.2	8.1	2.5

Plane and level of Measuring Point	K6	A7	D6	D8	F8	F10	A10	J10	A8	G6
Dim from Centre of Weld (mm) : x	31.7	0	9.6	9.1	15.6	15	0.1	27	0.2	19.3
Dim from Level 1 (mm): y	-25	-26	-25	-29	-29	-35	-35	-35	-29	-25
Dim from Weld Interface (mm)	26.7	1	4.6	4	4	10	10	10	4	14.3

Plane and level of Measuring Point	B7	D5	G5	K4	D3	D4	K3	D2	G2	A12
Dim from Centre of Weld (mm) : x	3.7	11.3	20.4	33.4	13.5	12.3	33.5	14.3	23.4	0
Dim from Level 1 (mm): y	-26	-20	-20	-15	-8	-15	-8	-3	-3	-40
Dim from Weld Interface (mm)	1	5.4	14.5	26.6	5.5	5.5	25.5	5.5	14.6	15

Table 2: Temperature measurement position from weld centre and weld interface (Reference point A1: (0,0)

with a spindle speed of 5000 rpm, axial load of 17.5 kN and a plunge depth 15 mm while a forging force equal to the axial force was applied for 20 s. As the weld progressed the transient temperatures were measured by each thermocouple.

3. Results

The platform process control data recorded during the welding is shown in figure 9 where the welding cycle can be divided into two process stages, a heat generating and a forging stage. During tool rotation, frictional heat is generated between the tool and work piece as well as between the subsequent shear layers formed in the plasticised third body material. At reaching the required consumed length of the tool, a downward force, or forging force is applied during which the plasticised third body material solidifies and cools down to form the finely grained weld plug material[20] . The cycle can further be divided into five secondary phases. Phase 1, the initial friction, or as sometimes referred to as "dry friction" (1) begins when the bottom surfaces of the rotating tool come into contact with the bottom of the hole. This causes a rapid rise in temperature at this point, resulting in an interface condition change from dry contact to contact between surfaces separated by a viscous layer of hot plasticised material. From figure 9 it can be observed that the measured process torque rises rapidly to an initial peak value in response to the dry friction before briefly settling at a slightly lower level. The second transient phase is identified by a stable torque and extends for 2.5 s to the point where the torque rise and cycles for a while before dropping-off, indicating the end of the third phase. During this third stage plasticised layers of the consumable tool are sheared off as the temperature reaches an optimum value for the plasticised third body material. This phenomenon is supported by the nature of the observed fluctuation in process torque and the related increase in burn off distance. The temperatures within these plasticised layers are high, therefore the shear resistance is relatively low, explaining the small fluctuation in process torque. Thus would spindle speed not have any significant influence on torque during this "steady state" phase, which is in agreement with other work done on

http://www.saimeche.org.za (open access) © SAIMechE All rights reserved.

friction welding and FTSW[13, 21]. As the layers spread across the interface, the resisting torque first increase then decreases before stabilising over the last 10 s. Phase 4 represents deceleration when the rotation is stopped and the torque value decreases to zero. The forging stage completes the weld as phase 5, during which the tool force (forging forge) is held constant for 20 s after which the weld process is complete. These trends are comparable to results reported by other researchers[6, 13].

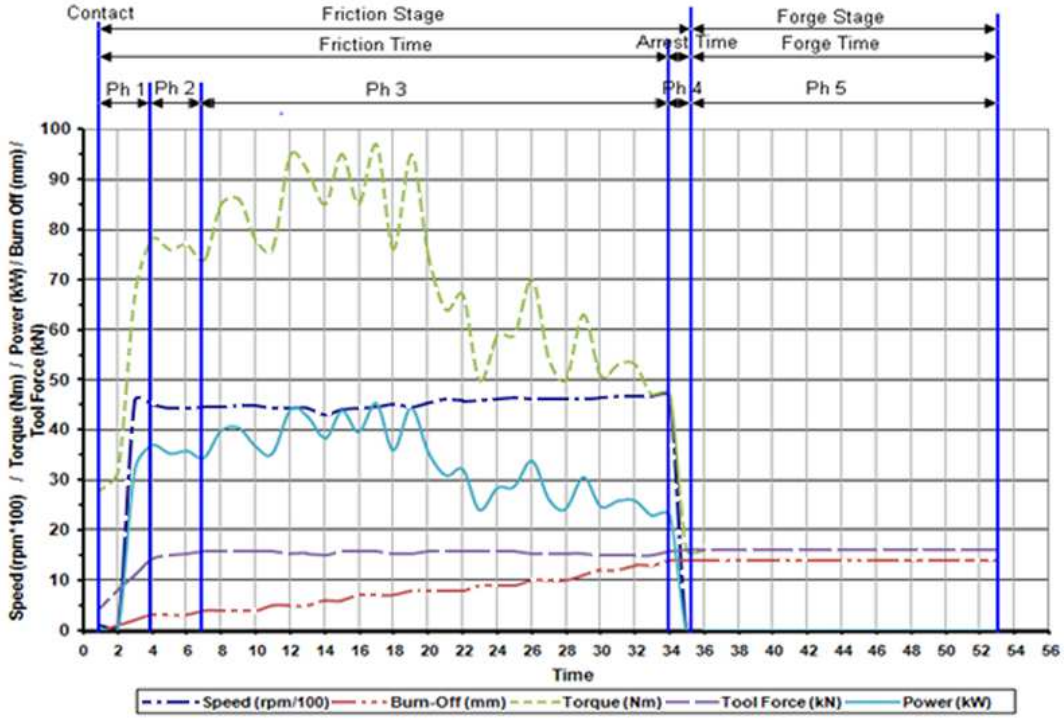

Figure 9: Schematic representation of FTSW process parameter behaviour

In figure 10, a macrograph of a section through the completed weld is superimposed on a schematic of the FTSW, illustrating thermocouple positions in relation to weld zones and flow of plasticised material as layers are moved up the hole.

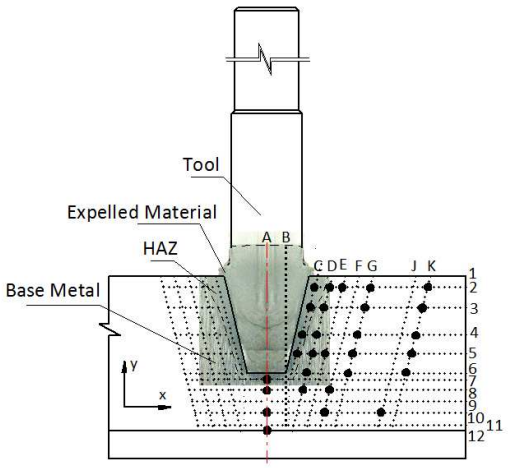

Figure 10: FTSW schematic with superimposed macrograph

The temperature profile of each thermocouple for the duration of the weld is graphically presented in figures 11 to 13, while the maximum thermocouple temperature, adjusted for time constant and calibration (which includes thermal transfer resistance) is shown in table 3. The time constant was found to be 0.638 s and the temperature adjustment made, allowing for a calibration error, was done by applying a polynomial equation shown in table 4.

The temperature lines show the maximum value measured and the rate of change in temperature for a specific measuring point during the weld. The power graph, as illustrated in figures 11 to 13, is fitted as a comparison between the input power and the true temperature profiles for each measurement position, as recorded. For clarity, 10 thermo-well positions are shown per graph.

http://www.saimeche.org.za (open access) © SAIMechE All rights reserved.

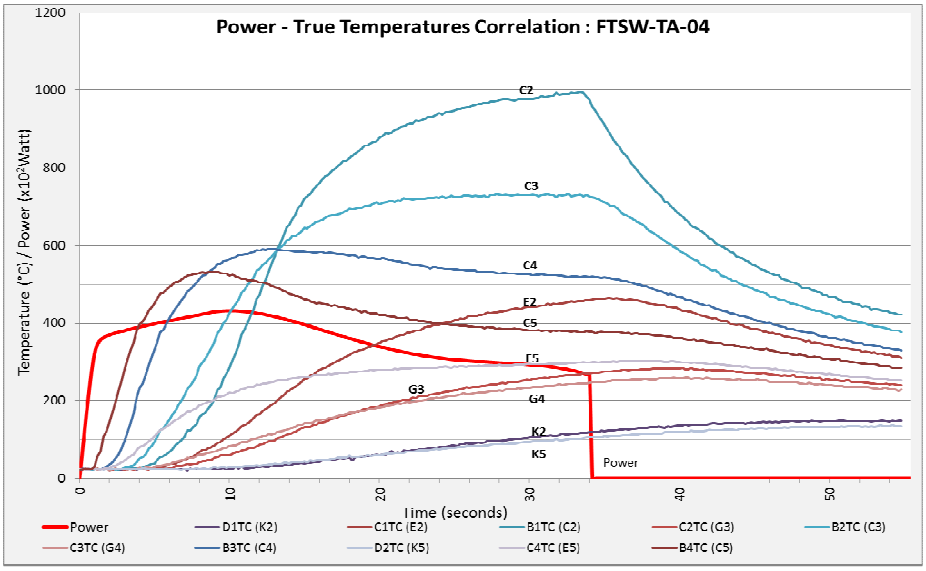

Figure 11: Temperature curve 1

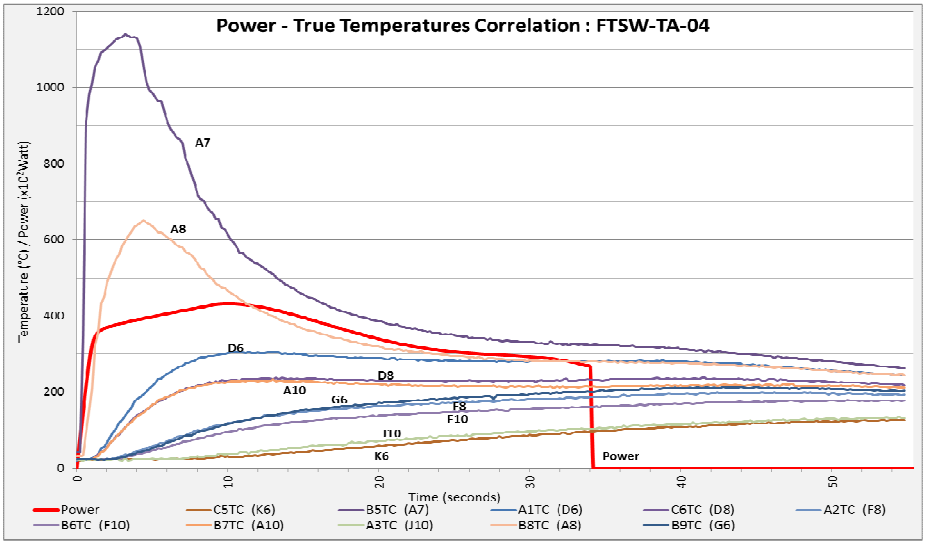

Figure 12: Temperature curve 2

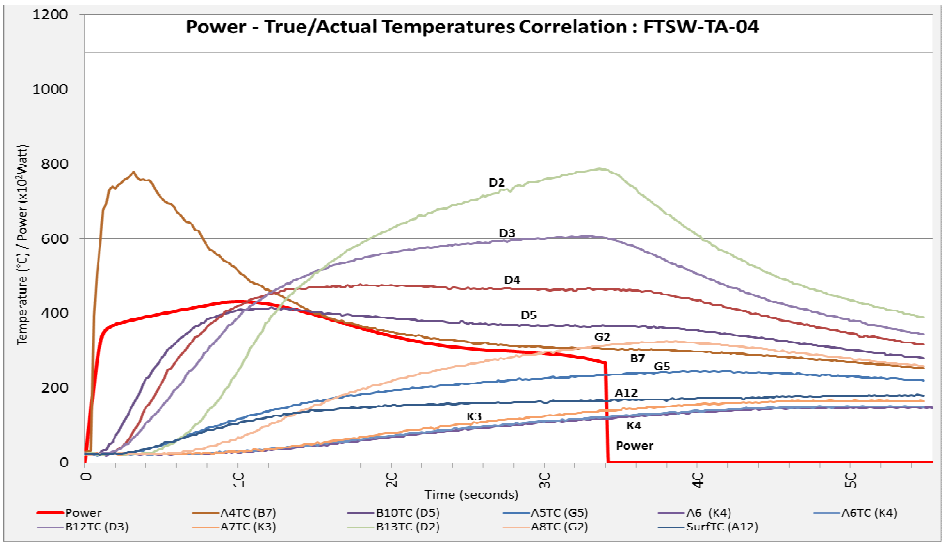

Figure 13: Temperature curve 3

Position	True Temp. (°C)	Co-ord (mm)	
		y	x
A7	1102	-26	0
A8	618	-29	0.2
A10	225	-35	0.1
A12	176	-40	0
B7	742	-26	3.7
C2	964	-3	11.2
C3	712	-8	10.7
C4	577	-15	9.2
C5	519	-20	8.4
D2	764	-3	14.3
D3	590	-8	13.5
D4	464	-15	12.3
D5	404	-20	11.3
D6	297	-25	9.6
D8	232	-29	9.1
E2	454	-3	17.2
E5	296	-20	14
F8	194	-29	15.6
F10	175	-35	15
G2	347	-3	23.4
G3	278	-8	22.6
G4	254	-15	21.2
G5	239	-20	20.4
G6	210	-25	19.3
J10	135	-35	27
K2	131	-3	34.3
K3	163	-8	33.5
K4	148	-15	33.4
K5	134	-20	32.1
K6	129	-25	31.7

Table 3: Maximum true temperatures

Temp (°C)	Error (°C)
0 - 200	-0.0015T+0.1167
200 - 1200	-0.0157T+2.94

Table 4: Thermocouple calibration error

Plane C together with points A7 and B7 are closest to the weld interface. The temperature profile of this near weld interface plane is indicated in figures 14 and 15 where the maximum measured temperature (1102 °C) was recorded after approximately 3 s at position A7, bottom centre and 1 mm from the weld interface. This is as expected and due to the heat generated by the initial dry friction between the two surfaces in contact and coincides with a peak in torque, at this position, where after the temperature steadily falls confirming the forming of a third body layer having a direct influence on the friction interface.

Position C2, 3 mm from the top surface and 2.4 mm from weld interface recorded the second highest value (964 °C) after 37 seconds as anticipated. It is believed that the expelled material, or flash at this position, has an influence on the temperature reached as it inhibits cooling by forming on the top surface of the weld coupon. From a weld time of approximately 5 s the temperature profile at the top of the weld (C2) starts increasing rapidly as heat is transferred from the viscous layer formed and continues with an upward trend until the end of the welding process. The middle of the weld (C4) shows a slight decrease in temperature from 11 s weld time onwards. After a rapid peak in temperature at around 3 s into the weld time, the bottom temperature profile (A7, B7) shows rather sharp cooling after which the temperatures stabilises at around 320 °C for the duration of the weld.

The temperature profiles, as distributed through planes within the parent material, is shown in figure 16 with reference to the positions of the thermocouple placements as per figure 8, at which points the maximum temperatures during the welding process were measured. Temperatures near the weld interface plane, on the outer wall of the weld, were found to be between 519 °C and 964 °C, with maximum weld temperature, 1102 °C, measured at the bottom centre of the weld interface and reducing in value to the perimeter at 742 °C.

4. Conclusions

The temperatures measured by the N type thermocouples were adjusted for calibration and time constant and these values were used as true temperatures measured. From this it can be accepted that the maximum temperatures at the said weld parameters were accurately measured. Because of the larger temperature gradients close to the weld interface, accurate placement of thermocouples in this region is critical. The results showed that the maximum temperatures of 1102 °C was recorded within 3 s from initial start, in the region of the bottom of the hole, during the initial 'dry' friction stage. The maximum temperature measured corresponded to about 70 % of the melting temperature of 10CrMo910. The next highest value of 964 °C was measured after 37 s (near weld completion) towards the top of the weld sample. Average weld power was found to increase rapidly at the beginning of the weld after which it tapered off towards the end as the third body material was plasticised. The power curve was derived from the torque applied and the shearing of layers can be seen in this curve. This is further supported by the trend in the tool consumption rate. It is the investigators opinion that process torque data should be measured more accurately and with greater care as it would allow for a proper interpretation of how the different shear layers are built-up. This temperature profile recorded was for a set of weld parameters and future work need to look at the influence of process parameters on peak recorded temperatures.

Acknowledgements

The assistance of Ian Wedderburn and the Automotive Components Technology Station at the Nelson Mandela Metropolitan University, Port Elizabeth, South Africa and Dr Axel Steuwer, University Lund Sweden is greatly appreciated. Mr Mark Newby and Phillip Doubell from ESKOM helped with assistance during experimentation, calibration of thermocouples and supply of test coupons. The NRF – IRDP and THRIP are thanked for financial assistance towards the project.

http://www.saimeche.org.za (open access) © SAIMechE All rights reserved.

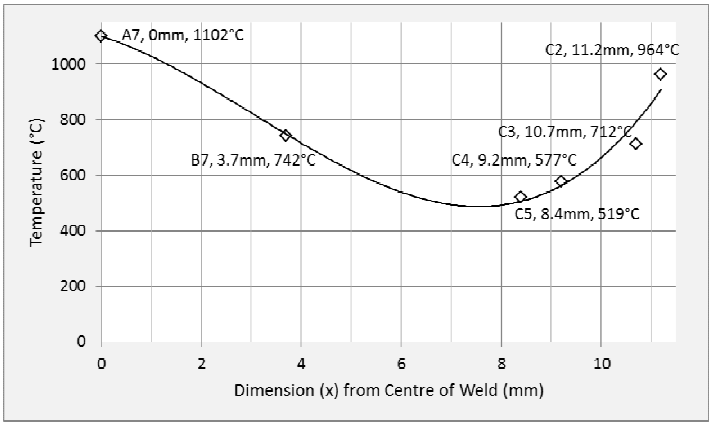

Figure 14: Maximum temperature profile: Near weld interface

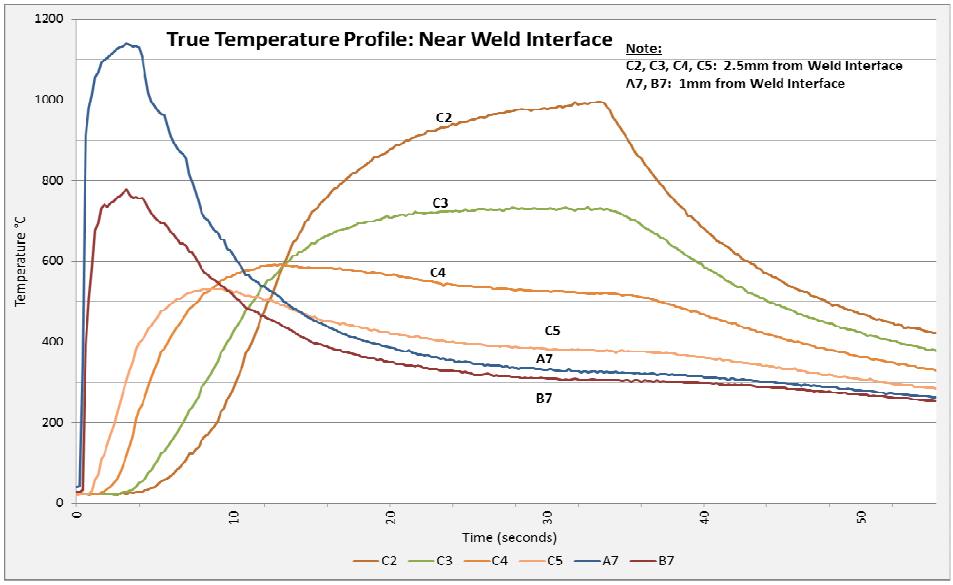

Figure 15: True temperature profile: Near weld interface

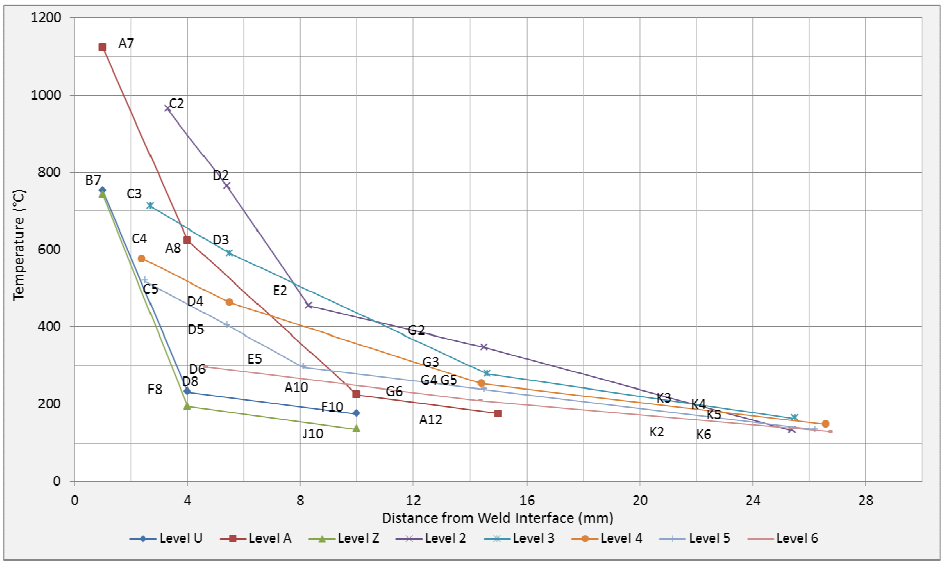

Figure 16: Temperature profiles

 © SAIMechE All rights reserved.

References

1. *Thomas W and Duncan A*, Friction based technology for joining and material processing - an introduction, Proceedings of 111 International Conference on Welding and Joining of Materials (ICWJM), 2010, Lima, Peru, http://www.twi.co.uk/technical-knowledge/published-papers/friction-based-technologies-for-joining-and-processing-september-2001/
2. *Vill V*, Friction Welding of Metals, Reinhold Publishing Corporation, New York, 1962.
3. *Suga Y, Miyakawa S and Ogawa K*, Estimation of temperature distribution in the friction welding of carbon steel by the finite element method, *Welding International*, 1999, 13(4), 262-269.
4. *Thomas W and Nicholas D*, Leading Edge: Friction Hydro Pillar Processing, TWI Connect, June 1992.
5. *Meyer A*, Friction Hydro Pillar Processing: Bonding mechanism and processing. Geesthacht: GKSS Forschungszentrum, Report No.: GKSS 2003/4, 2003.
6. *Pinheiro G*, Friction Hydro Pillar Processing of Lightweight Alloys: Bonding Mechanisms and Joint Properties, GKSS-Forschungszentrum, Institute of Materials Research, 2006.
7. *Thomas W and Nicholas E*, Emerging friction joining technology for stainless steel and alluminium applications, Productivity Beyond 2000, Asian Pacific Welding Congress, Auckland, 1996, http://www.twi.co.uk/technical-knowledge/published-papers/emerging-friction-joining-technology-for-stainless-steel-and-aluminium-applications-february-1996/
8. *Ambroziak A and Gul B*, Investigations of underwater FHPP for welding steel overlap joints, *Archives of Civil and Mechanical Engineering*, 2007, 7(2), 67-76.
9. *Thomas W and Nicholas D*, The need for gas shielding - positive advantages for two friction processes, *TWI Bulletin*, Sep/Oct 1997, 84-88.
10. *Nicholas D*, Friction processing technologies, *Advance Material Process.*,1999, 155(6), 69-71.
11. *Hattingh D, Doubell P, Newby M, Wedderburn I Steuwer A and James M*, Friction taper stud welding of creep resistant 10CrMo910 steel, *TMS 2009, Annual Meeting & Exhibition; Friction Stir Welding and Processing-V*, San Francisco, California, 2009, 75-84.
12. *Hattingh D, Steuwer A, James M and Wedderburn I*, Residual stresses in overlapping friction taper stud welds, Proceedings of MECA-SENS 5, 5th International Conference on Mechanical Stress Evaluation by Neutrons and Synchroton Radiation, Material Science Forum, Mito, Japan, 2010, 652.
13. *Bulbring D*, Characterization Of Friction Taper Stud Weld Properties As Applied To AISI 4140 High Tensile Steel, Masters Dissertation, School of Engineering, Nelson Mandela Metropolitan University, 2009.
14. AWS. Welding Handbook, 8th ed., American Welding Society, 1991.
15. *Frigaard O, Grong O and Midling OT*, A process model for the friction stir-welding of age hardened aluminium alloys, *Metallurgical and Materials Transactions* A, 2001, 32(5), 1189-1200, DOI: 10.1007/s11661-001-0128-4.
16. Chen C and Kovacevic R, Finite element modeling of friction stir welding - thermal and thermo-mechanical analysis, *International Journal of Machine Tools and Manufacturing*. 2003, 43(13), 1319-1326.
17. Yagi A, Hyde T, Becker A, Williams J, Sun W. Residual stress simulation in welded sections of P91 pipes. *Journal of Materials Processing Technology*, 2005, 167(2-3), 480-487.
18. AZoM - The A to Z of Materials, http://www.azom.com/article.aspx?ArticleID=5245 , 5 December 2010.
19. *Doubell P, Hattingh D, Wedderburn I and Lombard H*, Friction welding repair techniques for power plant, *Southern African Institute of Welding 60th Anniversary Conference*, (Published in "African Fusion", March 2009, 16-24); 2008; Gold Reef City, South Africa, 2008.
20. *Andrews R and Beamish K*, Characterisation Of, And Guidelines For, Rotary Friction Welding Of Common Metallic Engineering Materials, Report No.: 824/2005, TWI, 2005.
21. *Duffin F and Bahrani A*, Friction welding of mild steel, *Metal Construction and British Welding Journal*, 5(4), 125-132.

http://www.saimeche.org.za (open access) © SAIMechE All rights reserved.